DINAME 2023 - Proceedings of the XIX International Symposium on Dynamic Problems of Mechanics,
A.S. De Paula, A.T. Fabro and M.R. Machado (Editors), ABCM.
Pirenópolis, Go, Brazil, February 26th to March 3rd, 2023

Numerical hazard analysis of torque vectoring system for electric drivetrain considering handling uncertainty

Bruno A. Sorban[1], Maíra M. da Silva[2], Vinicius K. Marini[3], Roberto Bortolussi[4], Agenor T. Fleury[1] and Flávio C. Trigo[1]

[1] Escola Politécnica - USP

[2] Escola de Engenharia de São Carlos - USP

[3] Universidade Federal de Santa Maria - UFSM

[4] Faculdade de Tecnologia Santo André - FATEC-SA

Abstract: This work aims to perform a hazard analysis and a risk assessment considering vehicle handling and control when an electric drivetrain delivers power to the ground with the support of a torque vectoring control system. In addition, the objective is to discover pathways to dynamics control that allows the synthesis and implementation of devices that yield improvements to vehicle handling. The scope of the evaluation is to assess the impact of the tire dynamics' variability on a Formula SAE Electric Vehicle independently driven by rear in-Wheel motors. The context considers the tire dynamics' variability in coping with a torque vectoring strategy composed of feedforward and feedback signals. This strategy is derived using the simplest model for evaluating lateral vehicle dynamics, a bicycle model. However, the impact of the tire dynamics' variability is numerically assessed using a vehicle model comprising a TMEasy Tire model, suspension parameters, and the lateral transfer load. Numerical results demonstrate the importance of evaluating the specification to which vehicle systems are designed to ensure the safety of intended functionality by the system's components.

Keywords: safety of the intended functionality, torque vectoring, vehicle dynamics, electric vehicle

INTRODUCTION

Vehicles have been improving throughout the years in terms of speed and efficiency to deliver passenger and goods to places where needed. At the same time safety has risen as a significant concern in modern vehicle engineering, out of the understanding that engineering modern systems involve the responsibility for protecting life (Hammer, 1980). This perception evolved to become a value of modern society, which has driven improvements in driving assistance systems concerning support to dynamic control (Bengler *et al.*, 2014).

The transition of vehicle propulsion from internal combustion engines (ICE) to hybrid-electric drivetrain technology highlights the challenge of handling in the latter vehicles, since electric drives are less limited in power and can deliver it in full from idle (Ehsani *et al.*, 2005); thus, their engagement bears the risk of overwhelming the road-holding ability of the vehicle, which makes torque vectoring essential to control the vehicle safely. At the same time, uncertainties applying to its intended effect on handling or its ability to work at all may become vehicle-wide harmful safety issues.

The relationship of vehicle dynamics to safety is a shared characteristic of vehicle systems with early examples such as the Anti-lock Braking System (ABS) and the Traction Control System (TCS) (Bengler *et al.*, 2014). Torque vectoring comes as a further development of those early systems: in ICE vehicles, it helps directing engine power to control the vehicle (Sawase and Ushiroda, 2007); in electric vehicles, the integration of powertrain topologies with individual motors linked to the wheels can enable vehicle-wide systems to control single motors (Scheuch *et al.*, 2013)

We look forward to performing hazard analysis and risk assessment (HARA) of vehicle handling and control, by evaluating the actuators' limitation of a passenger vehicle (Saab 9-3 2.0T), considering it is driven by independent in-wheel motors by the rear. Aiming at this purpose, the method in this paper assesses the component's failure to cope with a torque vectoring strategy composed of feedforward and feedback signals. In the following section, the torque vectoring strategy is introduced. Both feedforward and feedback signals are derived using the simplest model for evaluating lateral vehicle dynamics, a bicycle (single track) model.

Next, a non-linear model of the vehicle is described. This non-linear model is used for evaluating the torque vectoring strategy considering the tire's non-linearities with the TMEasy Tire model (Rill, 2013), lateral transfer load, suspension parameters, and the tire dynamics' variability. The impact of the tire dynamics' variability is numerically assessed in the analysis section. This analysis is performed considering HARA to this vehicle's lateral behavior. Finally, conclusions are drawn based on these results.

VEHICLE SAFETY DEVELOPMENT CONTEXT

The commitment to developing modern vehicle systems to safety concerns is embodied in at least two instances: firstly, the *functional safety* approach in the ISO 26262 series (ISO, 2018a,; ISO, 2018b) addresses the emergence of hazards *when components fail to perform as intended*; then, the *safety of intended functionality* approach in the ISO/PAS 21448 specification (ISO, 2019a) addresses the emergence of hazards upon *whether required functionality is actually safe.* These standards provide directives to the design process regarding the delivery of safe vehicle systems.

Vehicle safety can be enhanced alongside the vehicle development process, as prescribed by the workflow represented in Fig. 1. Both ISO standards apply to the development process within the framework set by ISO 26262, to which the ISO/PAS 21448 prescriptions make a complementary set of activities. The procedure works in this manner because there is a scope delimitation between component failure modes arising from internal faults and critical scenarios arising from shortcomings in system functionality against triggering events from specific interactions between vehicle and environment (Saberi *et al.*, 2020).

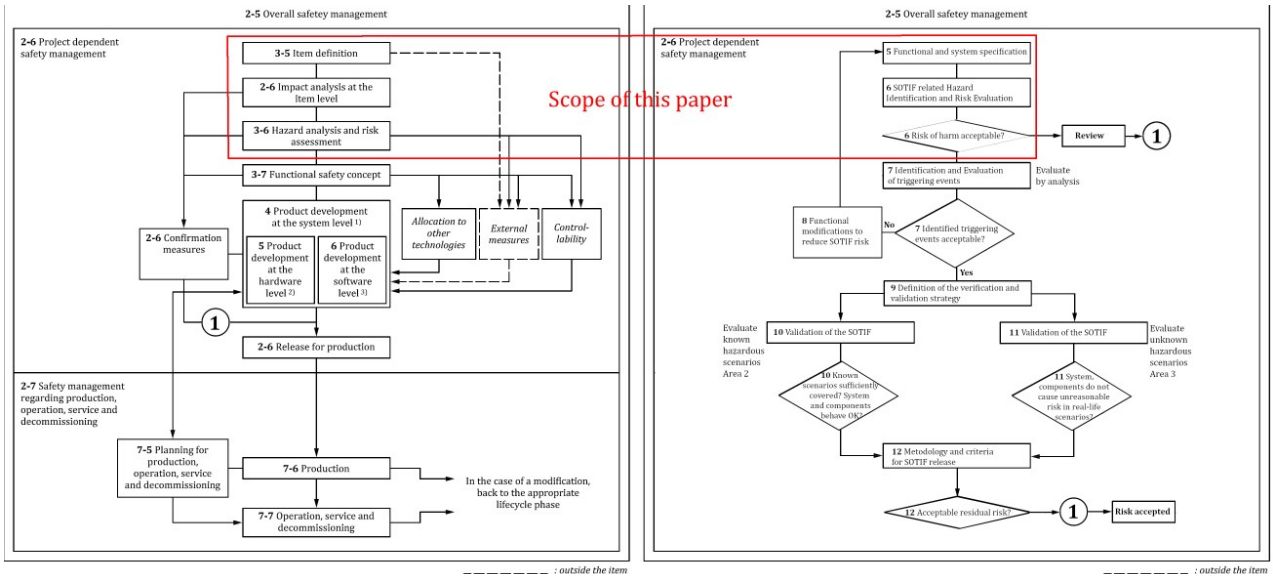

Figure 1: Development process framework for approaching and managing safety in vehicle systems. The prescriptive model for managing functional safety - left, based on (ISO, 2018b) - is complemented by a procedure for assessing safety of intended functionality - right, modified from ISO/PAS 21448 (ISO, 2019a).

These questions require engineers to be aware of considerations to vehicle dynamics: ISO 26262 deals with vehicle safety with attention to the functioning of its components and systems, and ISO 21448 approaches the subject from the viewpoint of whether design specifications of vehicle systems are sufficiently safe (Marini *et al.*, 2021). The complementary reasoning between both standards enables engineering teams to carry out a single subset of activities with focus on vehicle safety, supported by risk assessment methods (ISO, 2019b) to implement the proposed activities.

Table 1: HAZOP applied to the functional safety of a steering system, steering wheel hub (Becker *et al.*, 2018)

Guideword	Malfunction	Hazard
MORE	- Transmit more torque to steering column	- Unintended lateral motion - Unintended Yaw
LESS	- Transmit less torque to steering column than intended	- Insufficient lateral motion - Insufficient yaw
REVERSE	- Drivers' torque input is transmitted in opposite direction	- Unintended lateral motion - Unintended yaw

Among these methods, one that gains significant adoption for its versatility and simplicity is HAZard and OPerability (HAZOP) studies: Table 1 displays a HAZOP excerpt from a functional safety assessment on a passenger car steering system (Becker *et al.*, 2018). This is a functional analysis method that employs a critical examination in asking questions that reflect what would happen if certain deviations to intended system workings did happen. Its procedure departs from a statement expressing intended functionality and its target parameter, and relies on stating deviations whose effects should be considered (Kletz, 1997).

HAZOP places a significant design description requirement to engineers, because it depends on having information - including embodiment design - and expertise at hand regarding the deviations under consideration, and how much is actually enough to cause something wrong to happen (Marini *et al.*, 2010). Nevertheless, a hybrid analytical approach working with explicit design parameters can take advantage of the method, because fast computation times allow multiple runs to explore the parametric space and then find out the deviation effects as result.

TORQUE VECTORING DESIGN USING LQR AND A FEEDFORWARD SIGNAL

This work exploits the linear quadratic integral (LQI) control along with a feedforward signal for generating an input control for the direct yaw moment control u. Both control strategies are derived using a two-degree-of-freedom bicycle model shown in Fig. 2. This simplified model is frequently used for studying handling and stability characteristics during cornering maneuvers but presents limitations regarding the lateral load transfer and tires' non-linearities. Therefore, we evaluate this control approach using a more comprehensive non-linear model, detailed in the next section.

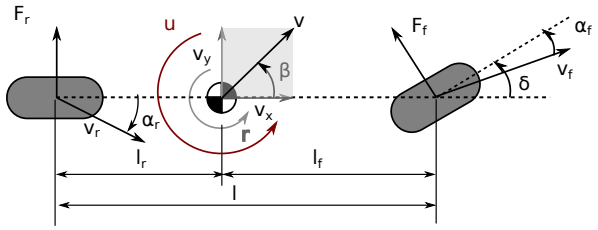

Figure 2: Simplified model for deriving the control: a 2-DOF bicycle model (modified from Wang *et al.*, 2018)

The motion equations applied to the bicycle model are (Wang *et al.*, 2018):

$$m(v_x\dot{\beta}+v_x r)=F_r+F_f \quad \text{and} \quad I_z\dot{r}=l_fF_f-l_rF_r+u, \tag{1}$$

where m is the vehicle mass, I_z is the mass moment of inertia, v_x and v_y are the longitudinal and lateral velocities, F_r and F_f are the rear and the front lateral tire forces, r is the yaw rate, β is the vehicle sideslip angle, and l_r and l_f are the distance between the rear/front tires to the center of mass (see Fig. 2). For the sake of control design, the lateral tires' forces are linearized as

$$F_f=C_{\alpha f}\alpha_f \quad \text{and} \quad C_{\alpha r}\alpha_r, \tag{2}$$

where $C_{\alpha f}$ and $C_{\alpha r}$ are the front and rear cornering stiffness. Side slip angles correspond to: $\alpha_f \approx \delta-\beta-(L_f r)/v_x$ and $\alpha_r \approx -\beta+(L_r r)/v_x$, in which δ is the steering angle. Based on these equations, one can derive the following state-space model:

$$\dot{\mathbf{x}}=\begin{bmatrix}\dot{\beta}\\ \dot{r}\end{bmatrix}=\begin{bmatrix}-\frac{C_{\alpha r}+C_{\alpha f}}{mv_x} & \frac{l_rC_{\alpha r}-l_fC_{\alpha f}}{mv_x^2}-1\\ \frac{l_rC_{\alpha r}-l_fC_{\alpha f}}{I_z} & -\frac{l_r^2C_{\alpha r}+l_f^2C_{\alpha f}}{I_zv_x}\end{bmatrix}\begin{bmatrix}\beta\\ r\end{bmatrix}+\begin{bmatrix}0\\ \frac{1}{I_z}\end{bmatrix}u+\begin{bmatrix}\frac{C_{\alpha f}}{mv_x}\\ \frac{l_fC_{\alpha f}}{I_z}\end{bmatrix}\delta=\mathbf{Ax}+\mathbf{B}u+\mathbf{E}\delta \tag{3}$$

$$\mathbf{y}=\begin{bmatrix}\beta\\ r\end{bmatrix}=\begin{bmatrix}1 & 0\\ 0 & 1\end{bmatrix}\begin{bmatrix}\beta\\ r\end{bmatrix}+\begin{bmatrix}0\\ 0\end{bmatrix}u+\begin{bmatrix}0\\ 0\end{bmatrix}\delta=\mathbf{Cx}+\mathbf{D}u+\mathbf{D_E}\delta \tag{4}$$

The torque vectoring functionality has to deliver a control strategy for u while the driver is delivering a steering angle δ. The control strategy in this work is composed of feedback and feedforward signals processed through the following controller design:

$$u=u_{lqi}+u_{ff}, \tag{5}$$

Figure 3 illustrates the intended control strategies. The feedback loop requires a state reference $\mathbf{x}_{ref}=[\beta_{ref} \quad r_{ref}]^T$ and an integral action on the error signal $r_{ref}-r$ where β_{ref} is the sideslip angle reference and r_{ref} is the yaw rate reference. The sideslip angle reference is null, while the yaw rate reference can be derived by the model (Wang *et al.*, 2018):

$$r_{ss}=\frac{v_x}{l(1+kv_x^2)}\delta, \tag{6}$$

where $k=m(l_fC_{\alpha f}-l_rC_{\alpha r})/(l^2C_{\alpha f}C_{\alpha r})$ is the understeer gradient. Equation 6 is a linear function of delta and the yaw rate; because of this, it can reach any value and that is unrealistic against the actual behaviour of such systems.

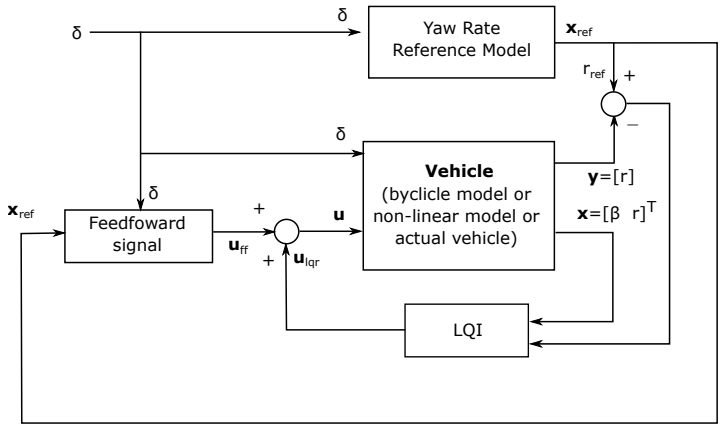

Figure 3: Feedback and feedforward strategies for the torque vectoring implementation

Therefore, a reference yaw rate model should take into account limitations due to the tyre-road friction interface, with considering $r_b = min(\|r_{ss}\|, c\mu g/v_x)sgn(\delta)$ (Li *et al.*, 2015), where μ is the friction coefficient and c is a safety factor ($c < 1$). In order to take into account delays regarding the system dynamics, a first-order filter is also applied for the generation of the yaw rate reference model yielding r_{ref}.

Both feedforward and feedback strategies are derived using the discrete-time state-space bicycle model. This model has been derived by using the zero-order hold discretization method yielding $\mathbf{x}_{k+1} = \mathbf{A}_d\mathbf{x} + \mathbf{B}_d[u \quad \delta]^T$. The feedforward signal is derived by assuming that $\mathbf{x}_{ref}$ and its derivative are given ($\beta_{ref} = 0$). Considering that the discrete derivative of r_{ref} is given by rd_{ref}, the u_{ff} can be derived as:

$$u_{ff} = Iz\big(rd_{ref} - \mathbf{A}_d(2,2)r_{ref} - \mathbf{B}_d(2,2)\delta\big). \tag{7}$$

The feedback control action is given by $u_{lqi} = [-\mathbf{K}\mathbf{x} - K_i(r_{ref} - r)]^T$, where the gains $[\mathbf{K}K_i]$ are derived by solving the LQI problem, which is based on the well-know LQR problem (Young & Willems, 1972). The non-linear model has been implemented in Matlab and is divided into five classes as shown in Fig. 4.

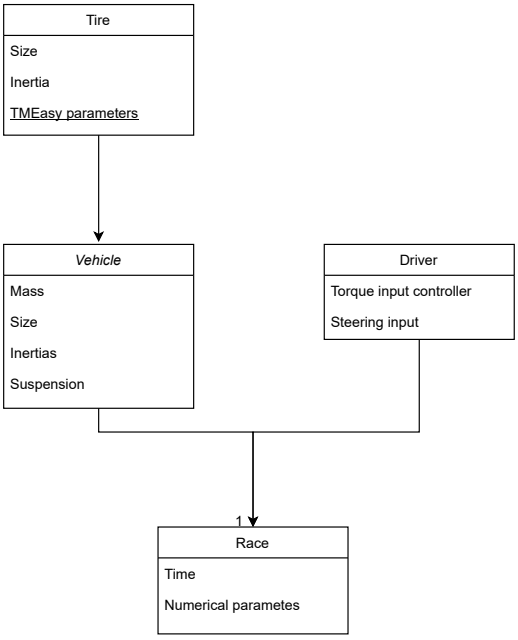

Figure 4: Vehicle dynamics model architecture

These classes are intended for collecting and organising the data flow, and their organisation enables modularizing the behaviour components of the vehicle model. The first one is *Tire* class, which contains an implementation of the TMEasy tire model (Rill, 2013). It is an input to the *Vehicle* class, which contains parameters including the mass, the center of gravity position, and axle track width. So far, it also contains the suspension parameters and functions that enable modelling the dynamic response of the vehicle. Along with a *Driver* class containing functions to calculate the control variables, the *Vehicle* class is an input to the *Race* class, which performs the integration of the equations of motion.

The lumped parameter approach presented in Balkwill (2018) works as basis to model the suspension in the *Vehicle* class. Figure 5 illustrates the vehicle's model with seven degrees of freedom: heave, roll, and pitch of the sprung rigid body and the vertical displacements of the unsprung masses (the tires). Balkwill (2018) assumes that each tire can be represented as an unsprung mass able to move vertically due to load transfer and ground displacement, as illustrated in Fig. 6(a). The dynamic behavior of each tire is obtained by exploiting the free-body diagram shown in Figure 6b.

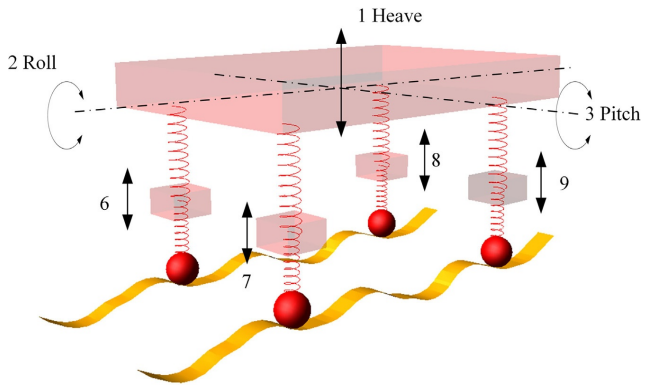

Figure 5: Lumped model of the non-linear vehicle used for assessing the vehicle's performance. Source: Balkwill (2018)

Several tire models are available in the literature. We use version 5.3 of the TMEasy model in this work (Rill, 2013). TMEasy is a semi-empirical tire model that is based on the brush model approach (Svendenius, 2007). This model considers the slip a three-dimensional parameter and provides a smooth transition between the stop condition and normal driving conditions (Rill, 2013).

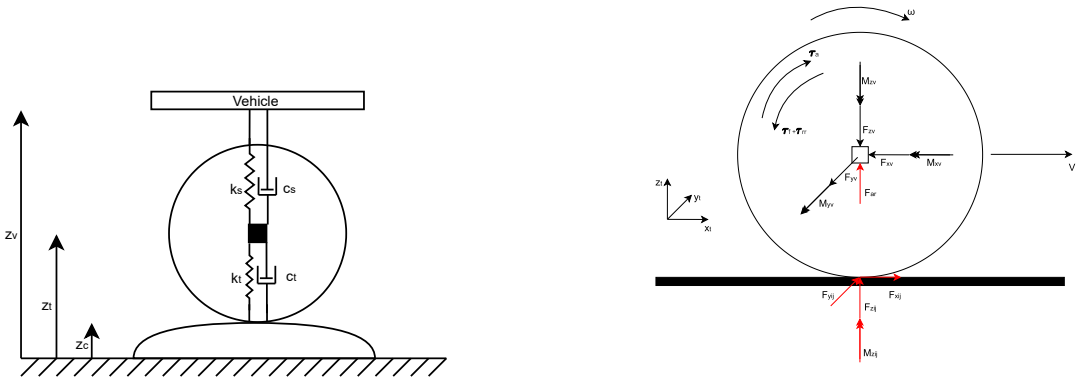

(a) (b)

Figure 6: Suspension Model: (a) Lumped model of the tire/suspension, and (b) Tire free-body diagram

The numerical results are derived from the aggregation of the routines shown in Figure 5 in considering that the vehicle moves on a flat, smooth road as a default condition. Moreover, we assume that the tires are always in contact with the ground and the camber angle is always null. Therefore, not all properties of TMEasy were implemented in the dynamic model, so for a complete view of the model, see Rill (2013). Details about the complete vehicle model considering non-linearities can be found in (Sorban, 2022).

DYNAMIC CONTROL ON A DOUBLE LANE CHANGE MANOEUVRE

The vehicle properties characterising the vehicle model for the dynamic control test are set from the parameters shown in Table 2, including the main properties of the Saab 9-3 passenger car, and its tyres (Fernandez, 2012). The vehicle behaviour is significantly influenced by its own weight distribution and its suspension setup. Besides the tires' size and their tread widths, their number of plies and cord angles make significant factors for their dynamic properties.

The class structure of vehicle models from Figure 4 is assembled for the purpose of providing simulation testbed towards assessing the dynamic behaviour of the vehicle in a severe condition where the algorithm is stressed in keeping control of the trajectory. The double lane change manoeuvre - 'moose test' - is implemented towards our control model through following the procedure set by ISO 3888-1 standard (ISO, 2018c). The intended distances the vehicle will run through the double lane change distances are illustrated in Fig. 7.

Table 2: Vehicle parameters (Fernandez, 2012)

Vehicle	Value	Unit	Tire	Value	Unit
Sprung mass (m)	1742	kg	Wheel width x size	7.5 x 17	inch
Track width (t)	1.517	m	Tread width	235	mm
Wheelbase (l)	2.67	m	Wheel mass, each	12	kg
Moment of inertia (I_z)	2617	kgm^2	Moment of inertia (I_z), each	1	kgm^2
Centre of mass location			Cornering Stiffness		
- from front axle (l_f)	1.07	m	- Front Tires (C_{α_f})	2100	N/deg
- from rear axle (l_r)	1.60	m	- Rear Tires (C_{α_r})	1750	N/deg

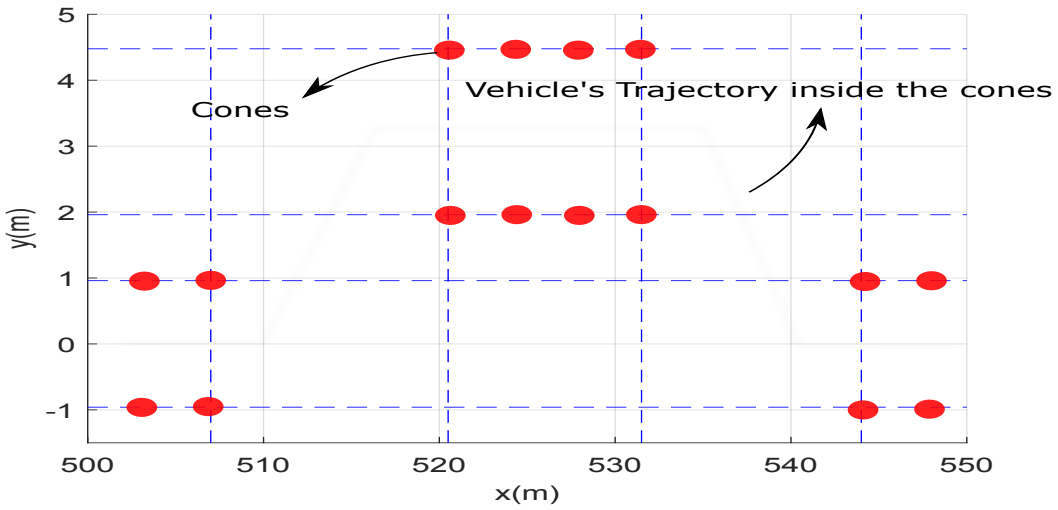

Figure 7: The double lane-change manoeuvre for passenger cars according to ISO 3888-1 (ISO, 2018c)

At the same time, the steering input for the control model to work is analytically prescribed through a hybrid sinusoid function, which is intended to provide a yaw rate reference function so that the control model shall keep the roadholding ability of the vehicle through the double lane change manoeuvre. In addition, the hypotheses of permanent road/tire contact on flat, clean and dry tarmac are adopted. The steering angle and the reference yaw rate functions, corresponding to the *Drive* class of the model architecture are shown in Fig. 8.

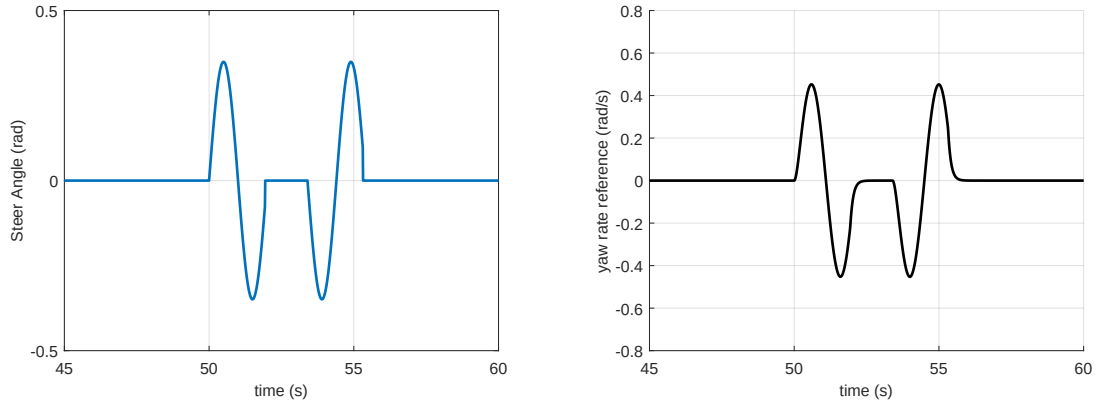

(a) (b)

Figure 8: (a) Steer Angle, and (b) Yaw rate reference for the double lane change

Figure 9 shows the combined tire forces profile, the self-aligning moment at selected lateral slip angles, and longitudinal/lateral forces at selected longitudinal/lateral slip angles for the Avon tire 6.2/20.0-13. However, the load and inflation pressure are the main factors affecting the cornering stiffness for a given tire. Two values for the vertical stiffness, 190000N/m and 133000N/m, which is highly dependent on the load and inflation pressure, are evaluated. This information corresponds to the *Tire* class shown in Fig. 4.

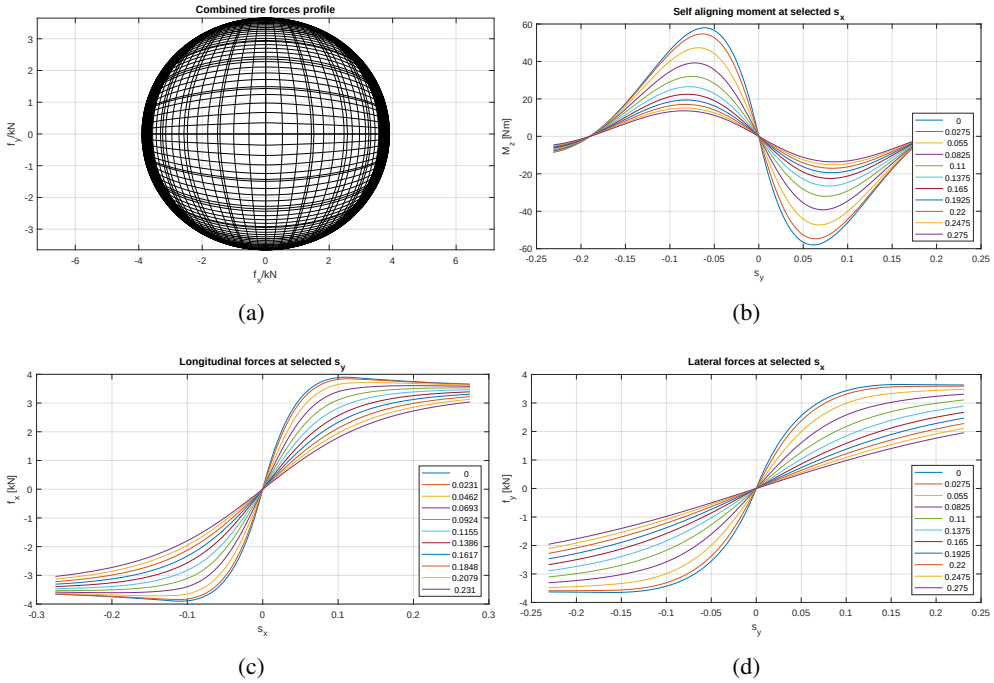

(a) (b)

(c) (d)

Figure 9: TMEasy tire model: (a) Combined tire forces profile, Self-aligning moment at selected lateral slip angles, (c) longitudinal forces at selected longitudinal slip angles, and (d) lateral forces at selected lateral slip angles

Figures 10(a) and (b) show the actual yaw rate and the reference yaw rate. The proposed controller is capable of tracking the yaw rate reference for both stiffness values. These results will show up effect in the trajectories the vehicle performs while undergoing the moose test manoeuvre.

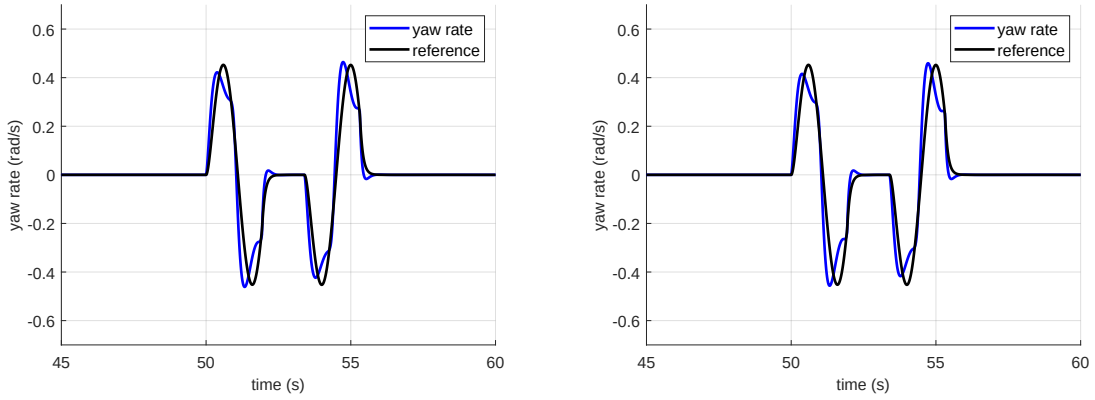

(a) (b)

Figure 10: Yaw rate reference and actual yaw rate for the vertical stiffness equals to (a) 190000 N/m, and (b) 133000N/m

Figures 11(a) and (b) show the feedforward (blue) and feedback signals (red) for both conditions. One can perceive that the feedforward values for 133000 N/m deviate further from the references than those for 190000 N/m. At the same time, the feedback signals present higher oscillations under a 133000N/m vertical stiffness, which suggests that the controller attempts to keep the vehicle under the yaw rate and sideslip reference values, with a higher control effort.

The deviations in yaw rate are especially significant by the first and the second yaw rate transitions, because the controller does not maintain the reference as trying to compensate for the steering direction changes in the manoeuvre. The actual yaw rate does also change sooner than the reference value, which indicates the effect of the feedforward signal into the steering control.

These deviations will manifest their result in the trajectory each vehicle setting undergoes through the moose test manoeuvre. A reduction in vertical stiffness does indeed affect the controller performance, forcing it to reduce its effect into compensating the variations in dynamic response from the vehicle. Preserving the simplification hypotheses stated for its execution, the vehicle architecture model enables the prediction of dynamic behaviour under severe manoeuvres.

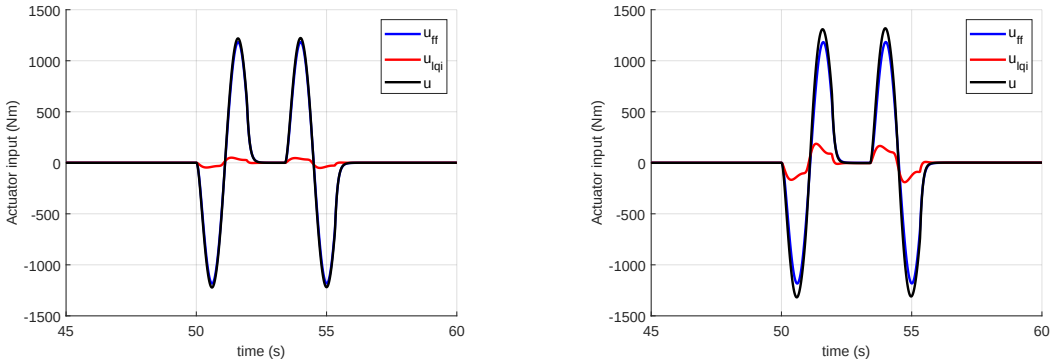

(a) (b)

Figure 11: Input signals for the vertical stiffness equals to (a) 190000 N/m, and (b) 133000N/m

HAZARD ANALYSIS APPLIED TO DOUBLE LANE CHANGE MANOEUVRE

The effects of vehicle stiffness changes will influence how the vehicle will perform the double lane change. The variations displayed in the feedback controller through Fig. 10 and Fig. 11 help exert the control actions required for successfully undergoing the manoeuvre. The vehicle undergoes the course of the manoeuvre with command from the same steering input function for both vertical stiffness scenarios, and displays variations in its ability to complete the course for each scenario.

Figure 12 shows that the vehicle running the course with a vertical stiffness equal to 190000N/m is capable of performing a double lane change manoeuvre within a maximum trajectory deviation of 110 mm sideways through the second straight. The steering input function is set to manage a bit of anticipation from the last cone location prior to the lane change, which enables adequate recovery in the second lane. The tyre drift that takes place by the second steering control is only compensated by the third steering movement, when driving back to the original lane.

This third steering movement manages to make the course back to the original lane without touching the cones. However, the steering input by the fourth movement does not fully correct the trajectory of the vehicle to a straight line parallel to the course, because of the tyre drift applying through the steering change. Nevertheless, a deviation of 438 mm sideways by the first 50m of the third straight line after recovering can be recovered with applying extra steering input.

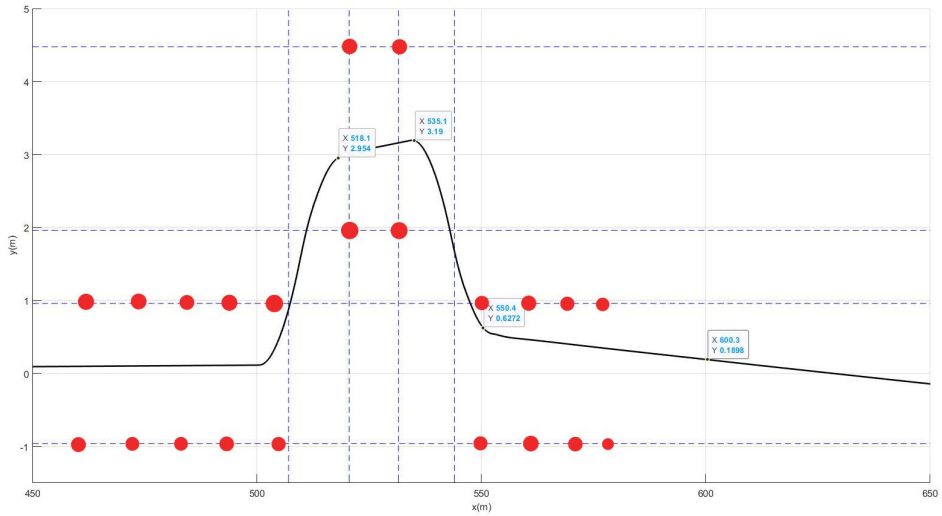

Figure 12: The double lane-change manoeuvre result for vertical stiffness equal to 190000 N/m

In contrast, Figure 13 shows the vehicle with a vertical stiffness value equal to 133000N/m isn't capable of performing the same manoeuvre. Under such conditions, it undergoes maximum trajectory deviation of 236 mm sideways through the second straight course. If such deviation isn't corrected by extra steering input applied in progressive manner, the vehicle may enter a situation where an usual traffic lane width isn't wide enough to accommodate for the deviation, thereby entering a stepwise ground level change by the shoulder lane and risking loss of control in this area.

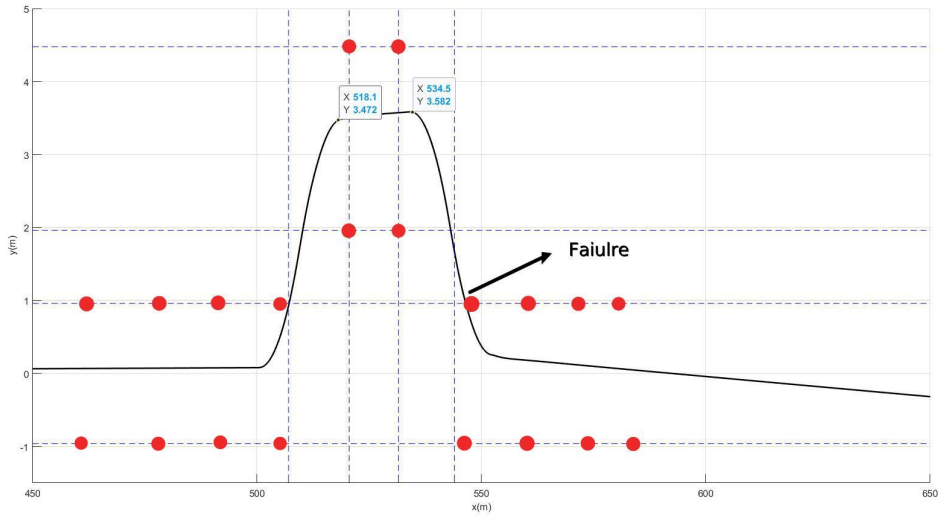

Figure 13: The double lane-change manoeuvre result for vertical stiffness equal to 133000 N/m

Considering that the vehicle is still going through the flat surface as assumed, the third steering movement has a reduced correction effect on the course of the vehicle in swerving through the cones. Hence, the vehicle drifts further afar so that it hits the first cone by the left at the original lane, where the steering input by the fourth movement tends to a further deviated course from the straight line. While such deviation seems to be still in reach of being corrected with extra steering, interference from the cone impact may actually induce the loss of control by the vehicle.

While the effects of different tire dynamics seem totally systematic by first looking at the results from an analytic/deterministic model, the comparison supports proper hazard identification and analysis through severe swerving manoeuvres. The change in vertical stiffness renders the vehicle unable to perform the required task with drifting away from its intended course and entering areas that are not available through usual traffic lanes, even if being as perfect as assumed for this algorithm test run.

CONCLUSIONS

Daily engineering practice brings us an awareness of the effect of parameter uncertainties (for instance, unbalanced mass distribution, and other unaccounted non-linear effects) and several kinds of disturbances caused by the environment (wind gusts, rain, traffic, and road conditions) to impair the torque control effectiveness.

According to the above results, the selection of a limited actuator for torque vectoring exposes the vehicle to a control hazard, thereby delivering an unsafe functionality. The design effort to solve this issue should focus on the enhancement of control capabilities from the system. Hence, it is possible to confirm our first statement on the importance of performing hazard analysis and risk assessment applied to the dynamic design of vehicle systems that comprise several physicals (mechanical, hardware) and logical (software) subsystems.

ACKNOWLEDGMENTS

We would like to acknowledge the Rota 2030 program enabling this and further studies with torque vectoring by independent traction motors.

REFERENCES

Balkwill, J., 2018, Performance vehicle dynamics. In: Balkwill, J. (Ed.). [S.l.]: Butterworth-Heinemann, ISBN 978-0-12-812693-6.

Bengler, K., Dietmayer, K., Färber, B., Maurer, M., Stiller, C. and Winner, H., ”Three decades of driver assistance systems: review and future perspectives”, *IEEE Intelligent Transportation Systems Magazine*, v. 6, n. 4, p. 6-22, doi: 10.1109/MITS.2014.2336271.

Becker, C., Nasser, A., Attioui, F., Arthur, D., Moy, A., and Brewer, J., 2018, ”Functional safety assessment of a generic electric power steering system with active steering and four-wheel steering features”, Report No. DOT HS 812 575, Washington, DC: National Highway Traffic Safety Administration

Ehsani, M., Gao, Y., Gay, S. E., Emadi, A., 2005, ”Modern electric, hybrid electric, and fuel cell vehicles: fundamentals, theory and design”, Boca Raton: CRC Press. ISBN 0-8493-3154-4

Fernandez, J. G., 2012, "A vehicle dynamics model for driving simulators", Division of vehicle Engineering and Autonomous Systems, Chalmers University of Technology.

Hammer, W., 1980, "Product safety management and engineering" Englewood Cliffs: Prentice-Hall, 324p. ISBN 978-0-93-987490-3.

ISO, 2018a, "International Standard ISO 26262-1: Road Vehicles – Functional safety – part 1: Vocabulary" Geneva: International Standardization Organization.

ISO, 2018b, "International Standard ISO 26262-1: Road Vehicles – Functional safety – part 2: Management of functional safety" Geneva: International Standardization Organization.

ISO, 2018c, "International Standard ISO 3888-1: Passenger cars — Test track for a severe lane-change manoeuvre — Part 1: Double lane-change" Geneva: International Standardization Organization.

ISO, 2019a, "Public Available Specification ISO/PAS 21448: Road Vehicles – Safety of the intended functionality" Geneva: International Standardization Organization.

ISO, 2019b, "Risk management — Risk assessment techniques" Geneva: International Standardization Organization.

Marini, V.K., Leonardi, F., Bortolussi, R., Fleury, A., Trigo, F.C., Mendes, A.S., Barreto, M.A.Z., 2021. "Evaluation of Platooning Control Model towards Safety of Intended Functionality with Basis on Operational Design Domain" *Proceedings of the 26th ABCM International Congress of Mechanical Engineering (COBEM 2021).* Florianópolis, Brazil.

Rill, G. 2013 TM-easy – a handling tire model based on a three-dimensional slip approach. *Proceedings of the XXIII International Symposium on Dynamic of Vehicles on Roads and on Tracks*, IAVSD 2013, Blacksburg, Virginia, USA.

Saberi, A.K., Hegge, J., Fruehling, T., Groote, J.F., 2020. "Beyond SOTIF: Black Swans and Formal Methods". *Proceedings of the 2020 IEEE International Systems Conference*, IEEE, Montreal.

Sawase, K., Ushiroda, Y., 2007, "Improvement of vehicle dynamics by right-and-left torque vectoring system in various drivetrains", *Mitsubishi Motors Technical review*, v. 20, p. 14-20.

Scheuch, V., Kaiser, G., Korte, M., Grabs, P, Kreft, F., Holzmann, F., 2013, "A safe torque vectoring function for an electric vehicle", *Proceedings of the 2013 World Electric Vehicle Symposium and Exhibition*, IEEE, Barcelona.

Svendenius, J, 2007. "Tire modeling and friction estimation. Department of Automatic Control", Lund Institute of Technology, Lund University.

Sorban, B.A., 2022. "Modelagem e simulação numérica da dinâmica de um veículo leve de transporte de passageiros – BR-Shuttle". Relatório final de Iniciação científica. Orientador Flávio C. Trigo.

Wang, Z.; Montanaro, U.; Fallah, S.; Sorniotti, A. and Lenzo B., 2018, "A gain scheduled robust linear quadratic regulator for vehicle direct yaw moment Control", *Mechatronics*, v. 51, p. 31-45, doi: 10.1016/j.mechatronics.2018.01.013.

Young, P.C.; Willems,J. C., "An approach to the linear multivariable servomechanism problem", *International Journal of Control*, v. 15(5), pp. 961–979.